On the Mechanics of Earthquake Afterslip

CHRIS J. MARONE[1]

Department of Geology, University of Melbourne, Parkville, Victoria
and Division of Geomechanics, CSIRO, Mt. Waverly, Victoria, Australia

C.H. SCHOLZ

Lamont-Doherty Geological Observatory and Department of Geological Sciences, Columbia University, Palisades, New York

ROGER BILHAM

Cooperative Institute for Research in Environmental Sciences, University of Colorado, Boulder

We propose a model for earthquake afterslip based on rate and state variable friction laws. In the model, afterslip is attributed to the interaction of a velocity-weakening region at depth (within which earthquakes nucleate) with an upper region of velocity-strengthening frictional behavior. The existence of this upper region is supported by independent seismologic observations and the results of laboratory friction experiments. In our model, afterslip is the result of relaxation of a stress perturbation within the velocity-strengthening region, which arises when an earthquake propagates into that region from below. We derive the stress perturbation and its decay from the friction constitutive law using a simple, 1 degree-of-freedom approximation for the elastic interaction between the fault and its surroundings. This approximation is based on thickness-averaged displacements and slip velocities within the velocity-strengthening region, which is assumed to slip as a rigid block. Coseismic and postseismic slip are coupled through the thickness-averaged stiffness k of the velocity-strengthening region. We assume k to be inversely proportional to the thickness of this region, which means that thicker velocity strengthening regions have a greater tendency to arrest coseismic slip. We model the afterslip-time histories of the 1966 Parkfield and 1987 Superstition Hills earthquakes and relate the model parameters to physical parameters which may govern the rheologic behavior of the faults. In accord with field observations, our model predicts (1) that afterslip on some faults scales with the thickness of the (unconsolidated) sedimentary cover and (2) that proportionally more afterslip occurs for earthquakes in which coseismic surface slip is small compared with coseismic slip at depth. Velocity-strengthening frictional behavior is to be expected for faults within poorly consolidated sediments and for those that contain significant gouge zones (about >500 m) within their shallow regions (<3-5 km). Combining our results with those of recent laboratory friction studies indicates that relatively young faults with little accumulated fault gouge should exhibit little afterslip.

INTRODUCTION

Surface slip from large earthquakes often continues subsequent to the earthquake for a period of a year or more. Such postseismic slip, or afterslip, was first documented in California following the 1966 Parkfield earthquake [Smith and Wyss, 1968] and has since been measured following several other large earthquakes (1968 Borrego Mountain [Burford, 1972], 1975 Lake Oroville [Clark et al., 1976], 1976 Guatemala [Bucknam et al., 1978], 1979 Imperial Valley [Harsh, 1982; Sharp et al., 1982], and 1987 Superstition Hills [Bilham, 1989; Sharp et al., 1989; Williams and Magistrale, 1989]). In detail, these measurements show that afterslip accumulates in discrete pulses (so called creep events) of a few to 10 mm in amplitude, which decay in frequency following the mainshock [e.g., Smith and Wyss, 1968; Bilham, 1989]. On a

longer time scale, afterslip accumulates roughly linearly with log time. This behavior is remarkably consistent for different faults suggesting that afterslip represents a fundamental physical process or property of fault zones.

From the point of view of earthquake mechanics, we would like to understand the afterslip mechanism as well as its significance in a broader context, for example, its relationship to the mechanisms of rupture nucleation and/or its influence on the relative proportions of coseismic and postseismic slip for a given earthquake. A number of models for afterslip and fault creep events have been proposed [e.g., Scholz et al., 1969; Nason and Weertman, 1973; Crough and Burford, 1977; Wesson, 1987, 1988; Sharp and Saxton, 1989]. Most of these have focused on creep events, showing that their steep onset and gradual decay is consistent with a power law or quasi-plastic rheology [e.g., Crough and Burford, 1977]. With the exception of Wesson's [1987] work, afterslip curves have been described by empirical relations, with little attention paid to the underlying physical mechanisms.

Wesson [1987] extended an approach used to model creep events and showed that the overall time dependence of afterslip could be explained by a "two-phase" fault composed of locked patches and patches with a quasi-plastic rheology. As with the models for fault creep, this rheology was assumed to result

[1]Now at Department of Geology and Geophysics, University of California, Berkeley.

from clay-rich fault gouge [e.g., *Nason and Weertman*, 1973]. Although Wesson's model fits afterslip curves, it involves ad hoc assumptions about the rheology and the spatial distribution of coseismic and postseismic slip, and it does not explicitly couple coseismic and postseismic slip. The fault zone is assumed to obey one constitutive law during coseismic slip and a different law during postseismic slip. These limitations may be overcome by using a rate and state variable constitutive relation for the fault zone [e.g., *Rice and Gu*, 1983]. In this case, coseismic and postseismic phenomena are directly coupled through transient stressing associated with the earthquake.

The purpose of this paper is to propose a mechanism for afterslip based on the rate and state variable frictional laws. The model is motivated by (1) the success of the rate/state variable constitutive laws in describing a wide range of observations from laboratory friction experiments [e.g., *Dieterich*, 1979, 1981; *Tullis and Weeks*, 1986; *Marone et al.*, 1990; *Wong and Zhao*, 1990] and natural faults [e.g., *Rice and Gu*, 1983; *Tse and Rice*, 1986; *Marone and Scholz*, 1988; *Stuart*, 1988; *Okubo*, 1989] and (2) by field and laboratory observations (summarized below), which indicate that the upper regions (< 3-5 km) of many well-developed natural faults exhibit velocity strengthening frictional behavior, i.e., frictional resistance increases with slip velocity.

CHARACTERISTICS OF EARTHQUAKE AFTERSLIP

Scholz et al. [1969] noted that afterslip of the 1966 Parkfield earthquake was restricted to the upper 4 km and suggested that it was the stable (aseismic) equivalent of aftershocks, each arising from brittle fracture of stress concentrations produced during the mainshock. Whereas aftershocks were concentrated at the ends of the rupture and below 3-5 km, afterslip occurred mainly within the central region and was restricted to the upper 4 km. *Crook* [1984] made a similar observation for slip subsequent to the 1979 Imperial Valley earthquake. He inverted geodetic measurements [e.g., *Crook et al.*, 1982] and found that afterslip occurred only within the upper 4-5 km. In Imperial Valley, this depth corresponds to the transition from poorly consolidated sediments (above) to basement rocks below [*Fuis et al.*, 1982], indicating that afterslip was restricted to the sediments. A similar relationship has been noted by *Burford* [1972] and *Williams and Magistrale* [1989], who reported that afterslip of the Borrego Mountain and Superstition Hills earthquakes scaled with the local sediment thickness. Furthermore, *Burford's* [1972] measurements and those of *Bucknam et al.* [1978] show an inverse relationship between coseismic and postseismic slip, with less afterslip occurring in areas of larger coseismic slip. Taken together, these observations imply a causal relationship between afterslip and the presence of poorly consolidated sediments, as originally suggested by *Smith and Wyss* [1968].

Although several authors have since noted this relationship, [*Burford*, 1972; *Sharp et al.*, 1989; *Williams and Magistrale*, 1989], only recently has there been an explanation for its underlying cause and its significance for the mechanics of afterslip. In connection with a model to explain the paucity of very shallow seismicity on some faults, *Marone and Scholz* [1988] pointed out that the correlation between afterslip and poorly consolidated sediments could be explained by the velocity-strengthening characteristics of such sediments, which was also the basis of their explanation for the upper seismicity cutoff.

Because this velocity strengthening region is a fundamental aspect of the present model, we summarize the laboratory and field observations in support of it. (1) Both background microseismicity in Imperial Valley and aftershocks of the 1979 earthquake show that seismicity is confined below 4-5 km [*Doser and Kanamori*, 1986]. This depth corresponds to a transition from poorly consolidated sediments to basement rocks [*Fuis et al.*, 1982], indicating that seismicity is restricted to the basement rocks. *Marone and Scholz* [1988] summarize several other examples in which an upper cutoff in seismicity is observed along faults that contain a well-developed gouge/breccia zone or are overlain by thick sediments. (2) Coseismic slip during the 1979 Imperial Valley earthquake decreased dramatically at about 5 km [*Archuleta*, 1984], such that little to no coseismic slip occurred within the sediments above 4-5 km. Although this combination of detailed fault kinematic data and crustal structure is unique, such an upward decrease in coseismic slip is also indicated by "buried slip", as commonly inferred from comparisons of seismic moment and coseismic surface offset [e.g., *Scholz et al.*, 1969; *Scholz*, 1972; *Agnew and Wyatt*, 1989; *McNally et al.*, 1989]. (3) Recent laboratory friction experiments on simulated fault gouge (unconsolidated sand) show velocity strengthening frictional behavior [*Marone et al.*, 1990], which implies inherently stable, aseismic slip [e.g., *Gu et al.*, 1984]. These results are in contrast to experiments showing velocity weakening behavior for bare rock surfaces or highly indurated gouge [e.g., *Dieterich*, 1979, 1981; *Biegel et al.*, 1989; *Tullis et al.*, 1989]. However, the experiments on unconsolidated gouge are a more appropriate analog for poorly consolidated sediments and fault gouge within the shallow regions of active fault zones.

The velocity strengthening characteristics of unconsolidated material offer an explanation for the above observations [*Marone and Scholz*, 1988]. Specifically, the upper cutoff in seismicity can be explained as a transition from unstable, velocity-weakening frictional behavior at depth to stable, velocity-strengthening behavior within the upper 3-5 km. This is to be expected for faults overlain by poorly consolidated sediments and for those that contain thick unconsolidated gouge zones at shallow depths. Alternatively, this upper stability transition could be explained by low normal stress at shallow depths [e.g., *Brace and Byerlee*, 1970]; however, the transition is only observed in association with faults within unconsolidated sediments or those that contain thick gouge zones. Intraplate faults, which tend not to have significant gouge zones, do exhibit shallow seismicity [*Marone and Scholz*, 1988]. In addition, the correlation between the upper seismicity cutoff in Imperial Valley and the contact between basement rocks and poorly lithified sediments argues for a rheological explanation of the stability transition. Finally, because velocity strengthening implies negative stress drop, poorly consolidated materials will tend to arrest dynamic rupture, in agreement with *Archuleta's* [1984] results showing a rapid reduction in coseismic slip at the base of the sediments in Imperial Valley. The process of rupture retardation results in a stress increase, due to velocity strengthening. As we show here, afterslip can be explained by relaxation of this stress perturbation.

THE MODEL

In accord with the above cited laboratory and modeling studies, a fundamental premise of the present model is that the fault rocks of the upper crust exhibit rate and state variable frictional behavior. Thus, their steady state frictional strength τ^{ss} varies with sliding velocity V and can be written [see *Rice and Gu*, 1983]

$$\tau^{ss} = \tau_* + (A-B) \ln(V/V_*). \tag{1}$$

Here, A-B is the friction rate parameter and τ_* is the strength for steady state sliding at velocity V_*. Equation (1) is derived from the constitutive relations given by *Rice and Gu* [1983], which are compact versions of those proposed by *Dieterich* [1979, 1981] and *Ruina* [1983] to model laboratory friction data. The constitutive relations are

$$\tau = \tau_* + A \ln(V/V_*) + B\psi, \tag{2}$$

$$\frac{d\psi}{dt} = -\frac{V}{D_c}[\psi + \ln(V/V_*)], \tag{3}$$

where ψ is a parameter characterizing the evolving state of the sliding surface and D_c is the characteristic distance over which ψ evolves. At steady state $\psi = -\ln[V/V_*)$, which upon substitution into (2) leads to (1). Transient stressing associated with rupture of a fault which obeys rate and state variable friction can be evaluated by combining (2) and (3) with an equation describing elastic interactions between the fault and its surroundings [e.g., *Rice and Gu*, 1983].

In our model, we consider an elastic lithosphere which contains a fault zone with a velocity strengthening (A-B > 0) region of thickness h overlying a velocity weakening region (Figure 1). Afterslip is the result of stress relaxation within the velocity strengthening region; the stress perturbation arising from the sudden increase in slip velocity (from the preseismic slip rate, V_0, to the coseismic slip rate, V_{cs}) associated with seismic rupture propagation into this region from below.

To evaluate the stress perturbation and relaxation process, we consider a single-degree-of-freedom approximation for the elastic interaction between the fault zone and its surroundings. From (1), the stress jump ($\Delta\tau$) produced by the increase in slip velocity is $\Delta\tau = \ln(V_{cs}/V_0)(A-B)$. We assume that stress relaxation, and thus afterslip, is governed by the constitutive properties of the fault zones' upper region (Figure 1) and elastic interactions between the fault and this region. The velocity-strengthening region is treated as a single block, and a thickness-averaged stress jump within this block is related to a thickness-averaged displacement through a stiffness $k=G/h$, where G is the shear modulus of the velocity-strengthening region and h is its thickness. Afterslip is thus driven by elastic strains within the velocity-strengthening portion of the plate (Figure 2). By using a thickness-averaged stiffness and considering only thickness-averaged slip within the velocity strengthening region, the problem is reduced to that of a one dimensional spring-slider, with spring stiffness k, subject to the coseismic velocity change at the load point (Figure 2). Elastic interactions between the fault and its surroundings can be written

$$\frac{d\tau}{dt} = k(V_1 - V) \tag{4}$$
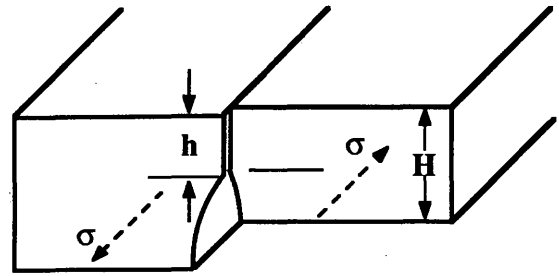
(a)
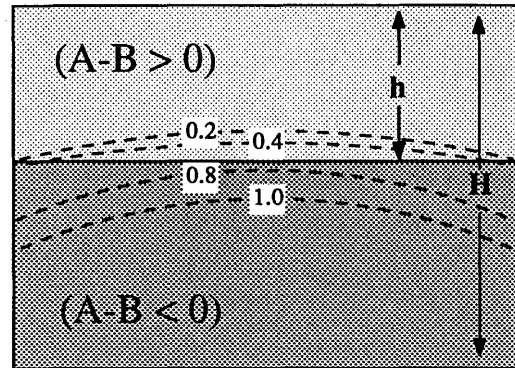
(b)

Fig. 1. Two layer model of the elastic lithosphere in which a velocity-strengthening region (A-B > 0) of thickness h overlies a velocity weakening region. The upper region is thought to be 3-5 km thick and represents the behavior of unconsolidated fault gouge/breccia or unconsolidated sediments. Earthquakes can only nucleate within the lower region. (*a*) Coseismic slip distribution showing thickness-averaged slip within the upper region. (*b*) Cross section along the fault plane; dashed lines show schematic contours of coseismic displacement for an earthquake at depth. Note that coseismic slip is suppressed within the velocity-strengthening region.

where V_0 is the load point velocity and k is the thickness-averaged stiffness for the velocity strengthening region (Figure 1).

The coupled equations (2)-(4) are solved numerically with $V_1=V_*$ to derive slip along the fault within the velocity-strengthening region. This treatment neglects the stress concentration within the upper region associated with approach of the rupture to the free surface (as in a model with a dislocation below a locked region). However, this is perhaps justified if the velocity-strengthening portion of the plate slips coseismically, at least in a thickness-averaged sense (e.g., Figure 1*a*).

Although the simplistic approach used to derive k has limitations, it (1) describes correctly the increased capacity to arrest coseismic slip of thicker velocity strengthening regions (Figure 1*b*), and (2) yields an inverse relationship between coseismic plate stiffness and h, as would be predicted by an elastic crack model in which, prior to rupture, shear stress within the plate is supported primarily along the portion of the fault that slips coseismically.

An alternative approach would be to use the stiffness given by *Tse et al.* [1985] for partially locked plate margins. In this case, treating the velocity strengthening region h (Figure 1*a*) as a slipped and unstressed region overlying a locked region to a depth H gives $k = (\pi G/2H) / \ln[2/(1+\cos(\pi h/H))]$ prior to
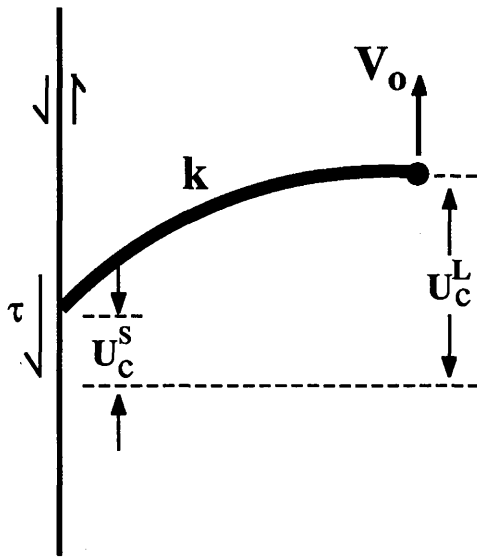
Fig. 2. Plan view showing thickness-averaged coseismic slip and thickness-averaged stiffness k within the velocity strengthening region. Displacement U^L_c represents coseismic displacement at the base of the velocity-strengthening region (or at a point sufficiently remote from the fault plane). The coseismic surface displacement along the fault is given by the thickness-averaged coseismic displacement U^s_c. To derive coseismic slip and afterslip for the velocity-strengthening region we use a single-degree-of-freedom spring-slider system. A massless slider is loaded through a spring of stiffness k by a point that moves at velocity V_0. The slider exhibits rate/state variable frictional behavior with velocity strengthening. By analogy, an increase in load point velocity represents an earthquake and coseismic slip at depth, whereas motion of the slider represents the (thickness-averaged) displacement along the velocity-strengthening portion of the fault. Because the slider exhibits velocity strengthening, energy is stored within the spring during coseismic slip and released via afterslip. In our model, k scales inversely with the thickness of the velocity-strengthening region.
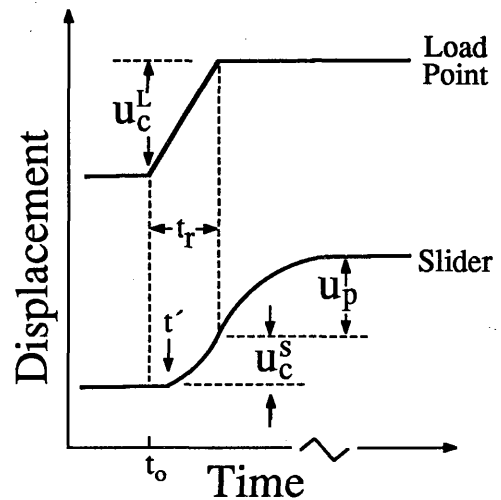
Fig. 3. Schematic displacement history for the seismic cycle as predicted by the spring-slider model (Figure 2). The load point velocity increases from V_0 (long-term creep rate) to V_{cs} (coseismic slip rate) at time t_0 for duration t_r, by analogy, producing coseismic slip at depth U^L_c. The slider, which represents the thickness-averaged surface response, undergoes coseismic slip U^s_c beginning at time $t' \geq t_r$, and postseismic slip U_p. See text for further discussion.

coseismic slip [*Tse et al.*, 1985]. With this relation, (1) k is inversely proportional to h and (2) the presence of the slipped region near the top of the plate tends to arrest dynamic rupture. However, *Quin's* [1990] dynamic modeling of the 1979 Imperial Valley earthquake shows that a negative stress drop is required in the upper region. The coseismic displacements above 5 km are overestimated by at least a factor of 2 if the upper region has zero stress drop as it would for the slipped region envisaged by *Tse et al.* [1985]. Furthermore, the stiffness given by *Tse et al.* [1985] differs from that we propose above by only a factor of 2-3 for h of 3-5 km and H=15 km and thus given its other limitations does not represent a significant advantage over the simpler form. Clearly, a more detailed model is needed to fully account for along-strike variations in slip and three-dimensional elastic interactions between the fault and its surroundings. However, this is beyond the scope of the present work.

Spring-Slider System as an Analog for the Seismic Cycle

We may regard motion of the spring-slider system as an analog to slip during the postearthquake portion of the seismic cycle, with the load point representing the velocity weakening region and the slider representing the velocity-strengthening region. Consider the displacement history shown in Figure 3. At time t_0, the slip velocity of the load point increases from V_0

to V_{cs} for a period t_r (by analogy, the rise time or coseismic slip duration) resulting in slip of the load point U^L_c (the coseismic displacement at depth). The slider undergoes coseismic displacement U^s_c (coseismic surface offset) beginning at $t' \geq t_0$, where U^s_c is a function of t_r and both U^s_c and t' are functions of the stiffness k and A-B; that is, U^s_c may be ≈ 0 for a sufficiently compliant spring or small value of t_r. At $t = t_0 + t_r$, the load point velocity returns to V_0 (coseismic slip ends) and the elastic strain stored within the spring is released via afterslip, U_p. This strain arises from the increased frictional resistance associated with velocity strengthening (e.g., Figure 4), as indicated by equation (1). Because the model ignores inertia and contains no dissipative terms, $U_p + U^s_c \to U^L_c$ as $t \to \infty$. Coseismic and postseismic slip are coupled and inversely related. For a sufficiently stiff spring, $t' \to t_0$, and the slider undergoes coseismic displacement $U^s_c = U^L_c$. From our relation for k, this is equivalent to a vanishingly thin
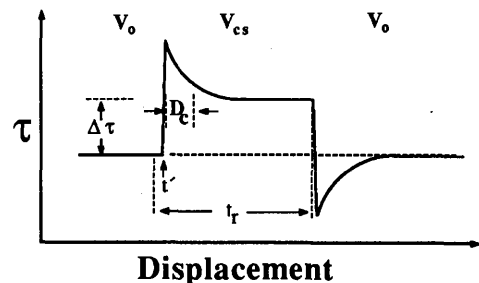
Fig. 4. Variation in frictional resistance with slip velocity for velocity strengthening. $\Delta\tau$ is the steady state increase in friction for a velocity jump from V_0 to V_{cs}. D_c is the characteristic distance over which friction decays following a change in load point velocity. t_r is the coseismic slip duration, and t' is the onset of coseismic slip for the slider (velocity-strengthening region). See Figure 3.

velocity-strengthening region, in agreement with the observation of large coseismic and small postseismic slip in areas where the alluvial cover is thin [e.g., *Burford*, 1972].

To illustrate the behavior of afterslip produced by the model, we show a model afterslip curve along with data from two earthquakes (Figure 5). The numerical afterslip curve is not intended as a direct simulation of the data. Rather we present the curve to show its general form for some typical parameters. The model was calculated using equations (2)-(4)and the following values: h=3 km, G=10 GPa, effective normal stress gradient (σ_n') =15 MPa/km, V_0=2 mm/yr, V_{cs}=0.2 m/s, t_r=0.5 s, D_c=10 mm, and a-b=0.005 where a-b=$(A$-$B)/\sigma_n'$. The preseismic slip rate V_0 is characteristic of central or southern California where V_0 is generally one tenth or less of the long-term plate velocity [e.g., *Schulz et al.*, 1982; *Louie et al.*, 1985]. The values of V_{cs} and t_r are consistent with *Archuleta's* [1984] modeling of the 1979 Imperial Valley event. The constitutive parameters are the laboratory values of *Marone et al.* [1990], except for D_c, which previous modeling indicates must be much larger for natural faults than laboratory samples [e.g., *Tse and Rice*, 1986; *Scholz*, 1988; *Stuart*, 1988; *Lorenzetti and Tullis*, 1989]. In general, the model afterslip curve is similar to the measured data, showing a steep onset followed by gradual decay 100-300 days after the mainshock. Varying individual parameters shows that afterslip is insensitive to D_c (postseismic displacement after 1 year varies by < 5% for D_c in the range 10 μm to 10 mm if coseismic slip U^s_c is greater than 2-3 times D_c) but depends fairly strongly on k, t_r, a-b, and the ratio V_{cs}/V_0.

It is instructive to consider variations in model afterslip with parameters such as coseismic duration, the constitutive parameter a-b, and the thickness of the velocity strengthening region (or k, since k=G/h). For given values of a-b, k, and V_{cs}/V_0 the ratio of coseismic surface offset to afterslip (U^s_c/U_p) should increase with rupture duration or U^L_c (roughly speaking, earthquake stress drop), since once the slider reaches a steady state frictional resistance during coseismic slip its velocity is V_{cs} and thus offset (U^s_c) accumulates rapidly, while the amount of afterslip is fixed by a-b, k, and V_{cs}/V_0. This is illustrated in
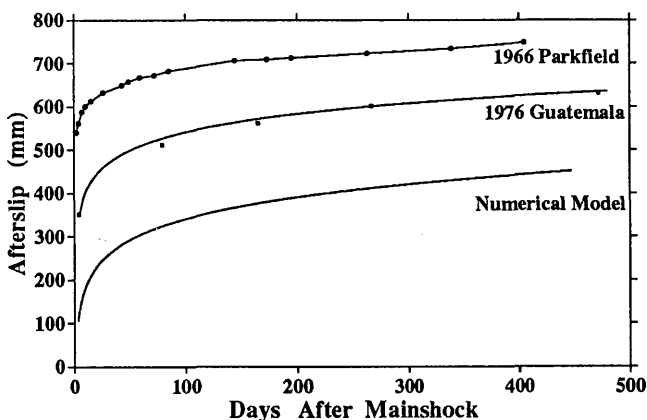

Fig. 5. Relative afterslip versus time for the numerical model and two earthquakes. The model is calculated using typical earthquake parameters (see text) and laboratory-derived values for the constitutive parameter (a-b). The general characteristics of the model curve agree well with the data, each showing a steep onset followed by a gradual decay in slip rate. Parkfield data are from Taylor Ranch [*Smith and Wyss*, 1968]. Guatemala data are from Zacapa [*Bucknam et al.*, 1978]. The line fit to the Guatemala data is that given by *Bucknam* et al.

Figure 6, which shows the relative proportions of coseismic and postseismic slip versus h for different values of t_r and a-b. Consider Figure 6a, the total slip of the slider 1 year after the mainshock (by analogy, coseismic surface offset plus afterslip) is composed almost entirely of coseismic slip for small h, since this corresponds to a very stiff spring in the spring-slider model. With increasing h, coseismic slip diminishes and afterslip increases, in agreement with field observations of reduced coseismic surface slip and increased afterslip where sediments are thicker [e.g., *Burford*, 1972].
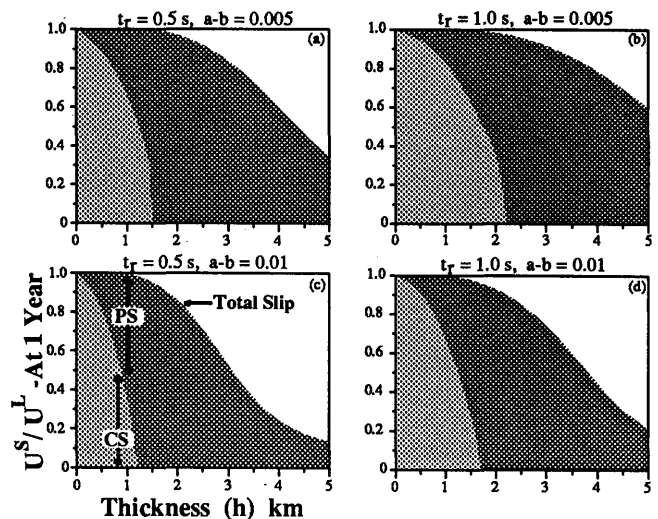

Fig. 6. Model calculations of the relative contributions of coseismic and postseismic slip to total surface offset (U^S) 1 year after an earthquake. U^S is normalized by the slip at depth (U^L). (a) and (b) The effect of coseismic duration (t_r) for a given a-b. (c) and (d) The effect of increasing a-b. In each case, thinner velocity-strengthening regions produce a greater proportion of coseismic slip relative to afterslip. For a given value of a-b, coseismic slip increases with rupture duration (Figures 6a and 6b). Coseismic slip and the total slip within 1 year decrease for greater velocity strengthening (Figures 6a and 6d).

For the model parameters of Figure 6a, velocity strengthening regions thicker than 1.6 km do not experience coseismic surface offset. For large h, afterslip decreases and the total slip of the slider at 1 year is significantly less than that of the load point (by analogy, slip at depth). This is simply because the stiffness becomes very low; the remaining slip would occur as postseismic slip after 1 year. For longer rise time the ratio U^s_c/U_p increases for smaller h, and, in general, a greater proportion of the total slip occurs within the first year after the mainshock (Figure 6b). Increased velocity strengthening (larger a-b) results in a smaller amount of both coseismic and postseismic slip (Figures 6c and 6d). Thus the total slip at 1 year decreases with the degree of velocity strengthening.

Analytical Approximation of the Afterslip Model

Although the spring-slider system reproduces measured afterslip and is useful for examining the mechanics of our model, it requires a numerical solution. This is troublesome from the point of view of fitting the model to data and recovering parameters that might be used to evaluate the model (e.g., the constitutive parameters, which may be compared with laboratory values, or the depth h, which may be compared

with geologic or seismically derived estimates). We therefore introduce the following closed-form solution for afterslip (given by Scholz [1990]):

$$U_p = \frac{A\text{-}B}{k} \ln\left[\left(\frac{kV_{cs}^{S}}{A\text{-}B}\right)t + 1\right] + V_0\, t.$$

(5)

A derivation of (5) is given in the appendix; the symbols have the same meaning as above with the exception of V^s_{cs}, which is the thickness-averaged coseismic slip velocity within the velocity strengthening region. Note that V^s_{cs} is expected to be less than V_{cs} [Archuleta, 1984]. As in the numerical model, equation (5) is based on rate/state variable friction and the idea that afterslip is the result of relaxation of a stress perturbation produced by dynamic rupture propagation into a velocity-strengthening region. This relation is valid if the velocity-strengthening region reaches a steady state friction level during coseismic slip (i.e., for a thickness-averaged slip greater than D_c, as shown in Figure 4).

We may evaluate limitations of the analytical approximation by comparing equation (5) with the numerical model for some typical parameters (Figure 7). To simplify the comparison, we make use of the following: (1) much of the available afterslip data fall within the range 1 day to 1 year, (2) the measurements are often relative to some fixed points installed after the mainshock, and (3) due to creep events, afterslip measurement can only be considered accurate to ±4 mm for the purposes of fitting the overall behavior; that is, a creep event could have occurred just prior to or just after the measurement. Given these limitations, we need only compare equation (5) and the numerical solution for t <1 year and for relative afterslip. (Note that the primary reason for this restriction is to simplify the comparison; the analytical approximation agrees well with the numerical solution after 1 year and in an absolute sense.) Figure 7a shows that equation (5) reproduces the numerical model well.

Similar comparisons were made for a range of the parameter values $a\text{-}b, D_c$, h, etc. (Table 1). An example is shown in Figure 7b, which shows the effect of varying $(a\text{-}b)$ from 0.005 to 0.015. The curves have been offset and plotted versus log time to allow comparison of the afterslip rate. As with the lower $a\text{-}b$ value, the closed form solution reproduces the numerical solution well. For the range of $a\text{-}b$ values considered, the maximum difference in relative afterslip for t < 1 year is 5 mm; this occurs for $a\text{-}b=0.005$ and represents about 2% of the slip that occurred between 1 day and 1 year. Table 1 also shows that varying the characteristic friction distance D_c does not degrade the agreement between the two models. The only case in which significant disagreement arises is for small values of h, and this is due to the lack of a term for continued fault creep [in addition to afterslip] in equation (5). That is, for thin velocity-strengthening regions, the thickness-averaged stiffness $(k=G/h)$ becomes large, resulting in very little afterslip. In the numerical model, this means that the slider resumes slipping at the long-term creep rate within a few tens of days, whereas (5) shows essentially no slip after this time. The difference becomes significant for h < about 1 km (using the other values indicated in Table 1) and thus it may be appropriate to include a term $V_0 t$ in equation (5) for fault zones with little overlying sediment or which contain little unconsolidated gouge/breccia. We note that for the central section of the San Andreas fault it takes about 1-2 years for the

postseismic slip rate to reach the long-term creep rate [Nason, 1973; Schulz et al., 1982; Wesson, 1987], so at least in this case the omission of the $V_0 t$ term is not significant. We may conclude, then, that from the point of view of fitting available afterslip data, the numerical model and equation (5) are essentially identical.

COMPARISON OF THE MODEL WITH DATA

One way to evaluate our afterslip model is to treat the parameters in equation (5) as free variables and determine how well the relation fits afterslip data. However, in addition, because (5) is derived from a physical model, we can also compare the values so obtained with independent estimates; i.e., laboratory measurements in the case of $a\text{-}b$ or seismic data in the case of V_{cs} and h. If the model is to be considered successful, the values derived from a least squares fit to the data must agree with the constraints imposed by independent measurements.

We fit afterslip data from two earthquakes using a "two-variable" version of equation (5):

$$U_p = \alpha\, \ln\left[\left(\frac{\beta}{\alpha}\right)t + 1\right],$$

where $\alpha=(A\text{-}B)/k$ and $\beta=V^s_{cs}$. We first consider afterslip data for the 1966 Parkfield earthquake. Data from five sites were fit, in a least squares sense, using an iterative nonlinear curve-fitting technique (Table 2). The data and site locations are from Smith and Wyss [1968]. The sites are listed in Table 2 from south to north; Carr Ranch is 15 km north of the southernmost extent of surface rupture, and Classen Ranch is at the northernmost end of surface rupture (21 km north of Carr Ranch). The errors indicate reasonably certain values for α and less certainty in β. The large relative uncertainty in the values for Classen may be attributed to having fewer data points there (7) than for the other sites (10-12) and because measurements began there 50 days after the mainshock, compared to 2-10 days for the other sites. Curves generated using equation (5) and the data from Table 2 show good agreement with the afterslip data (Figure 8), and thus at the least, equation (5) is capable of describing measured afterslip data.

We may now compare the model parameters (Table 2) with independent estimates. From the above relation, $\alpha=\sigma_n{'}(a\text{-}b)/k$, which for a given lithostatic gradient results in a relation between $a\text{-}b$ and k or the thickness of the velocity strengthening region (Figure 9). The $a\text{-}b$ values are plotted on a log scale to expand the region 0.001-0.005, which represents the range of relevant laboratory measurements [Marone et al., 1990]. For sites within the Parkfield area, the α value for the laboratory range of $a\text{-}b$ indicates a 2-4 km thick velocity strengthening region, in agreement with estimates of the depth distribution of afterslip ($\approx$ 4 km [Scholz et al., 1969]) and an estimate of h based on the upper cutoff in seismicity (3-4 km [Marone and Scholz, 1988]).

The modeling also provides an estimate of the V^s_{cs}, via β, which is the thickness-averaged coseismic slip velocity within the velocity-strengthening region. However, evaluation of equation (5) shows that afterslip is only sensitive to V^s_{cs} during the first few hours to 1/2 day following the mainshock. After 1 day the relative afterslip is insensitive to V^s_{cs}. Thus, unless the absolute offset is known (which it is not for the
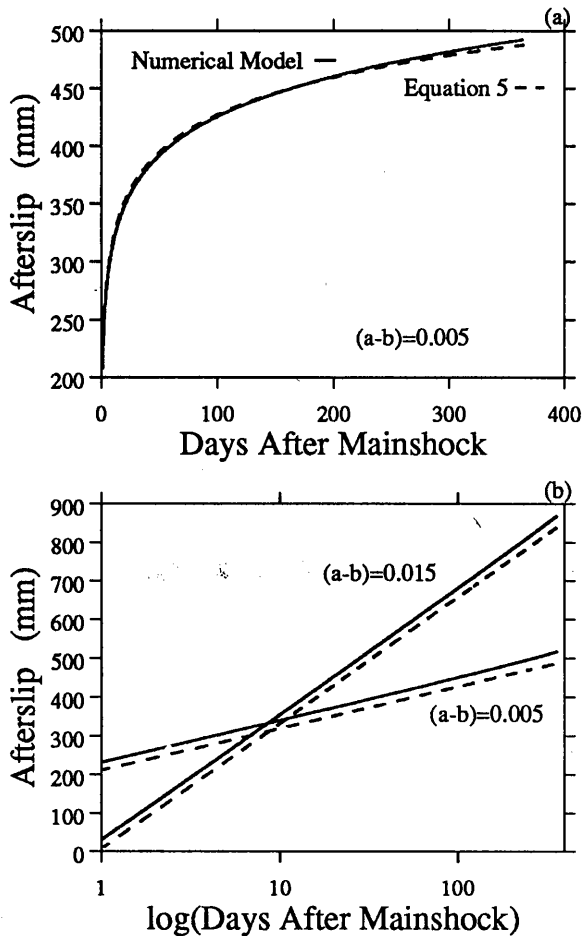
Fig. 7. Comparison of the numerical and analytic solutions for afterslip. (a) The relative afterslip from 1 day to 1 year is plotted and shows good agreement (see Table 1 for the parameter values used). (b) The data from Figure 7a are offset to facilitate comparison and plotted versus log time. Increasing the value of a-b does not degrade the agreement between the two solutions.

TABLE 2. Afterslip Modeling; 1966 Parkfield Earthquake

	α, mm	β, mm/day
Carr Ranch	27.64 ± 1.56	190.6 ± 53.5
Peacock Ranch	38.03 ± 0.79	91.5 ± 8.9
Taylor Ranch	39.38 ± 0.51	162.7 ± 9.9
Parkfield City	36.94 ± 1.06	107.4 ± 13.9
Classen Ranch	50.08 ± 5.64	7.8 ± 2.2

Values for least squares fit of equation (5) to afterslip data; uncertainties are 1 s.d., $\alpha=(A-B)/k$ and $\beta=V^s_{cs}$. Data are from Smith and Wyss [1968].

Figure 4, $\Delta\tau$ represents the excess shear stress arising from increased slip velocity and velocity strengthening. In connection with the modeling of Quin, $\Delta\tau$ arises as a negative stress drop within the upper 4-5 km, which is required to reproduce the slip distribution of Archuleta [1984]. That is, in
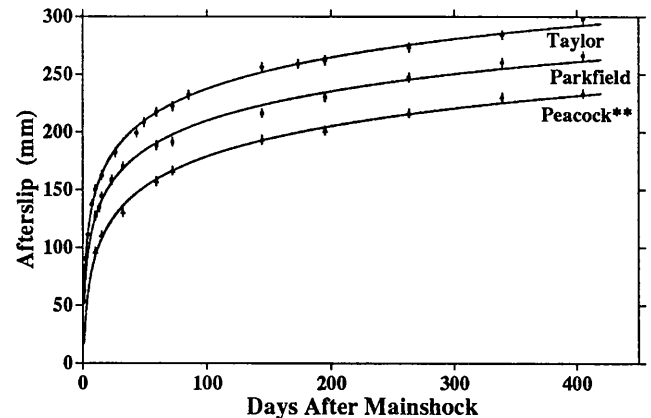

Fig. 8. Comparison of afterslip measurements with curves generated using equation (5) and the parameters given in Table 2. Error bars are ±4 mm. Data from Smith and Wyss [1968].
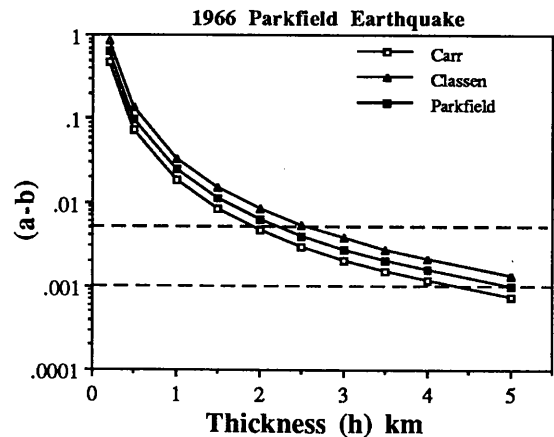
Parkfield event) or relative measurements begin immediately after the mainshock, the β values are unreliable. The values in Table 2 are significantly lower than those given by laboratory experiments or seismic modeling, which are 0.01-0.5 m/s $(8.64\times10^2\text{-}4.32\times10^4$ mm/d) [Johnson and Scholz, 1976; Okubo and Dieterich, 1984; Archuleta, 1984]. Nonetheless, it is worth noting that V^s_{cs} provides an estimate of $\Delta\tau$, via equation (1), which may be compared with that derived from dynamic rupture modeling [e.g., Quin, 1990]. As indicated in

TABLE 1. Comparison of Numerical and Analytical Solutions for Relative Afterslip

	L, mm	V_o, mm/yr	h, km	$(a-b)$,
Range Studied	10-50	0.2-20	0.5*-5.0	0.005-0.015
Max. Misfit	3 mm, <1%	2 mm, <1%	1 mm, <1%	5 mm, 2%

Misfit is maximum difference between equation (5) and numerical model for times < 1year; this difference is also given as a percentage of relative slip between 1 day and 1 year. Each parameter was varied independently, with the others held at L=10 mm, V_o=2 mm/yr, V_{cs}=0.1 m/s, h=2.5 km, a-b=0.005, $\sigma_n{}'$=15 MPa/km.

*For h < 1km the comparison was made over the afterslip duration (and not 1 year), since afterslip gives way to (long-term) fault creep before 1 year.

Fig. 9. Plots of the constitutive parameter $a-b$ versus thickness of the velocity strengthening region. The curves are defined by the parameter α, which is derived from fitting equation (5) to afterslip data (see Table 2). Laboratory measurements of a-b are in the range 0.001-0.005 (dashed lines), and thus the curves indicate a velocity strengthening region 2-4 km thick, in good agreement with independent estimates. The plot is made by substituting $k=G/h$ in the definition of α (see text), which after rearranging yields a-$b = (\alpha G)/(\sigma_n{}' h)$; we use $\sigma_n{}' = 15$ MPa/km.

order to reproduce the sharp upward decrease in coseismic slip, the dynamic modeling requires a retardation of rupture, i.e., a negative stress drop, which Quin's modeling indicates is 2-3 MPa. This can be compared with the initial driving force for afterslip $\Delta\tau$ arising from the stress increase associated with rupture into a velocity strengthening region. Using the V^s_{cs} values given by our modeling (Table 2) and the a–b values from Figure 9 and assuming $V_0 = 2$ mm/d, we obtain a relationship between $\Delta\tau$ and h (Figure 10). Our $\Delta\tau$ estimates are about a factor of 2 lower than those of Quin [1990].
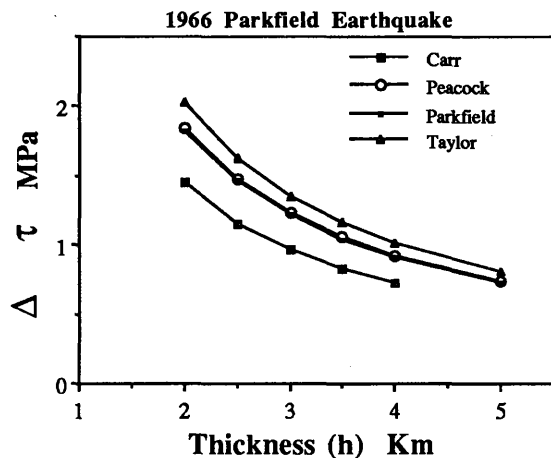
1966 Parkfield Earthquake

Fig. 10. The stress perturbation ($\Delta\tau$) associated with dynamic rupture into a velocity strengthening region is plotted versus the thickness of that region. The plots are made using the relation $\Delta\tau = a-b\ \sigma_n'$ $\ln(V^s_{cs}/V_0)$. The values of V^s_{cs} and a–b are given by fitting equation (5) to afterslip measurements, note that $V^s_{cs} = \beta$ (see Table 2). We used the a–b values from Figure 9 and $V_0 = 2$ mm/d.

A similar analysis was made for slip subsequent to the 1987 Superstition Hills earthquake (Table 3). Unlike at Parkfield, reliable measurements of absolute surface offset are available from several sites, and investigators combined these measurements with measurements of continuing afterslip [Sharp et al., 1989; Williams and Magistrale, 1989]. Because of the large offsets measured only a few hours after the mainshock, equation (5) was modified to allow for the possibility of coseismic surface rupture. Thus, in addition to fitting the data with equation (5), we fit the data with the relation

$$U_p = U_c^s + \alpha'\ \ln\left[\left(\frac{\beta'}{\alpha'}\right)t + 1\right],$$
(6)

where U^s_c is the coseismic surface rupture and α' and β' have the same meaning as α and β (note the distinction, since in fitting the data with U^s_c, α, and β the latter parameters are expected to differ from those in equation (5)). As above, the parameters were obtained from a best fit to the data and the values were compared with independent measurements.

Comparison of the parameters for fits with and without the coseismic slip term (compare α', β' with α and β, Table 3) shows that the α term changes very little but that β is significantly smaller when the coseismic slip term is included. This is in accord with the finding that β is most sensitive to slip during the first 1/2 day or so, and thus controls the absolute level of the afterslip curve whereas α controls the time dependence of slip after about 1 day. Including the coseismic slip term substantially improves the fit to the data (Figure 11), however, in some cases (e.g., site 2U, Figure 11) significant misfit remains. As discussed below, this may be the

TABLE 3. Afterslip Modeling; 1987 Superstition Hills Earthquake

Site	α, mm	β, mm/day	α', mm	β', mm/day	U^s_c, mm	Distance (N), km
124[*]	18.14	5.85×10^3	22.30	8.0	108.4	1.5
	± 0.83	± 2.22×10^3	± 0.70	± 1.3	± 2.2	
156[*]	54.25	3.29×10^4	53.45	302.2	240.8	7.2
	± 0.70	± 3.93×10^3	± 1.08	± 264.0	± 42.3	
168[*]	63.06	1.14×10^5	64.93	224.3	383.8	9.5
	± 0.80	± 1.43×10^4	± 0.74	± 42.0	± 11.9	
1R[†]	60.45	6.86×10^4	62.77	623.6	271.6	11.8
	± 3.61	± 3.83×10^4	± 2.44	± 508.4	± 42.2	
2M[†]	60.71	4.98×10^3	65.70	140.1	194.1	15.5
	± 1.40	± 7.93×10^2	± 1.80	± 47.3	± 15.8	
2T[†]	61.55	3.46×10^4	65.69	518.1	237.1	18.6
	± 0.67	± 2.67×10^3	± 1.25	± 115.3	± 11.3	
270[*]	59.69	3.54×10^4	64.60	156.9	303.1	18.6
	± 1.17	± 5.75×10^3	± 0.88	± 26.0	± 7.9	
271[*]	73.46	1.05×10^4	78.73	107.7	316.1	19.0
	± 5.42	± 5.23×10^3	± 2.12	± 38.0	± 21.6	
2U[†]	65.39	6.84×10^3	73.67	249.2	181.5	19.1
	± 1.63	± 9.53×10^2	± 3.29	± 105.0	± 20.2	
277[*]	35.07	1.05×10^4	37.53	52.7	176.3	21.5
	± 0.96	± 2.25×10^3	±0.43	± 10.4	± 6.3	
284[*]	21.57	1.96×10^3	21.72	294.2	40.1	22.5
	± 0.33	± 2.06×10^2	±0.77	± 1127.4	± 79.4	

Values for least squares fit of equations (5) (α and β) and (6) (α', β', and U^s_c) to afterslip data; uncertainties are 1 s.d. The distance from the north end of the surface rupture is given for each site; total surface rupture length is 24.5 km [Sharp et al., 1989].
[*]Data from Sharp et al. [1989].
[†]Data from Williams and Magistrale [1989].
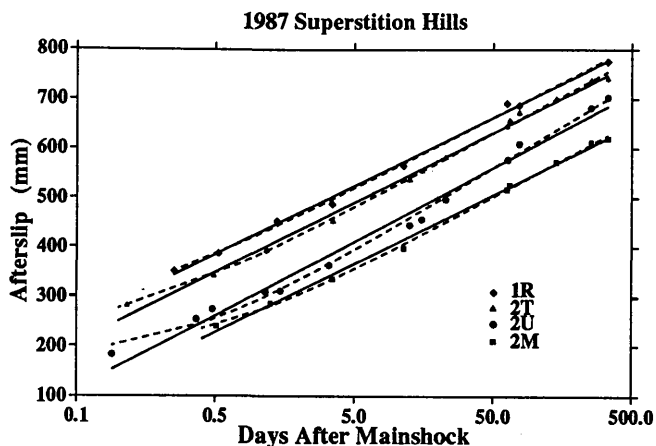
1987 Superstition Hills

Fig. 11. Comparison of afterslip measurements with curves generated using equations (5) (solid line) and (6) (dashed line) and the parameters given in Table 3. Note that the fit is improved by including the coseismic slip term $U^s{}_c$ (dashed line). Error bars for the data are on the order of the symbol size. Data (and site references) from *Williams and Magistrale* [1989].

result of slip triggered by the Elmore Ranch earthquake in addition to afterslip from the Superstition Hills event.

Figure 12 shows the a-b values implied by the α values for the Superstition Hills event (Table 3). For the range of laboratory a-b values, the modeling indicates a velocity strengthening region 2.5-5 km thick for sites within the central portion of the surface break, in excellent agreement with the seismic refraction work of *Fuis et al.* [1982], which shows a 3-5 km thick layer of sediments overlying the Superstition Hills fault and the area to the east. The α values are lower for sites near the end of the surface break, which is
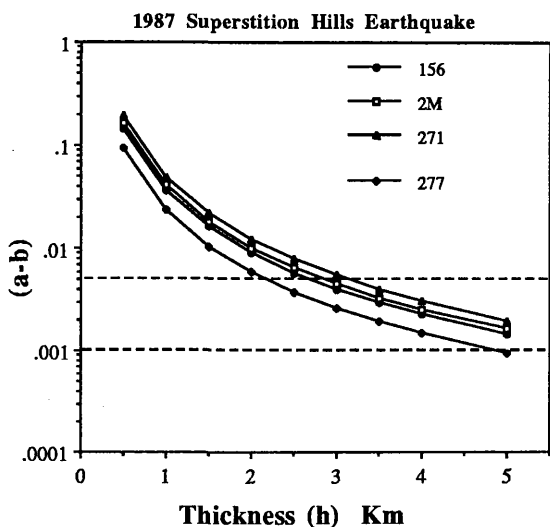
1987 Superstition Hills Earthquake

Fig. 12. Plots of the constitutive parameter a–b versus thickness of the velocity strengthening region. The curves are defined by the parameter α, which is derived from fitting equation (5) to afterslip data (see Table 3). Laboratory measurements of a–b are in the range 0.001-0.005 (dashed lines), and thus the curves indicate a velocity strengthening region 2.5-5 km thick, in good agreement with independent estimates. The plot is made by substituting k=G/h in the definition of α (see text), which after rearranging yields: a–b = $[\alpha$ $G]/(\sigma_n{}'\ h)$; we use $\sigma_n{}'$ = 15 MPa/km.

consistent with reduced slip at the ends of the rupture. The difference between α and α' and the errors in each are small relative to differences between sites, and thus including the coseismic slip term does not significantly alter the values of a-b or h (Figure 12).

As indicated above, the afterslip curves are very sensitive to β within the first few hours to day, and thus we expect that including $U^s{}_c$ results in a significant decrease in β (Table 3). The thickness-averaged coseismic slip velocities given by β (without the $U^s{}_c$ term) are in good agreement with *Archuleta's* [1984] kinematic modeling for the nearby 1979 Imperial Valley earthquake and laboratory measurements [*Johnson and Scholz*, 1976; *Okubo and Dieterich*, 1984]. However, given the data in support of coseismic surface rupture [*Williams and Magistrale*, 1989; *Agnew and Wyatt*, 1989] and the improvement our fits show when $U^s{}_c$ is included (Figure 11), we favor using β for $V^s{}_{cs}$, even though the values are somewhat lower than those of Archuleta [1984]. As above, these values can be used to estimate $\Delta\tau$ (Figure 13). The data for h=2-5 km show good agreement with those given by *Quin's* [1990] dynamic modeling.
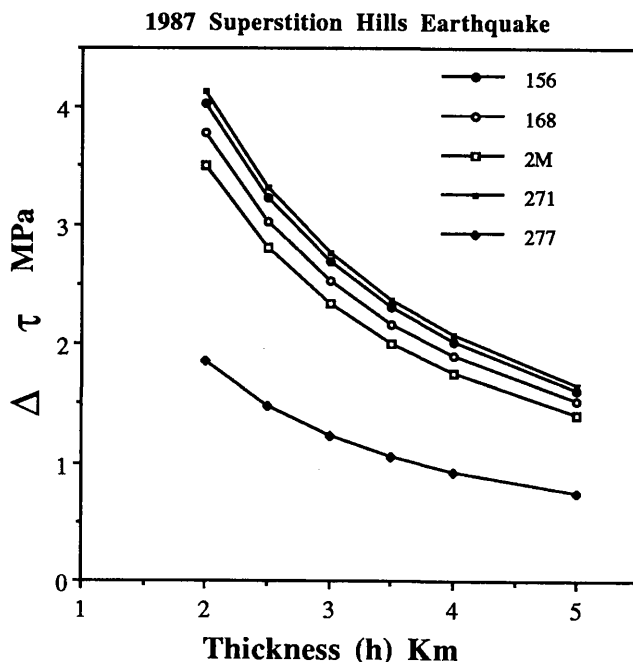
1987 Superstition Hills Earthquake

Fig. 13. The stress perturbation ($\Delta\tau$) associated with dynamic rupture into a velocity strengthening region is plotted versus the thickness of that region. The plots are made using the relation $\Delta\tau = a$–$b\ \sigma_n{}'$ $\ln(V_{cs}/V_o)$. The values of $V^s{}_{cs}$ and a–b are given by fitting equation (5) to afterslip measurements, note that $V^s{}_{cs}$ = β (see Table 3). We used the a–b values from Figure 11 and the preseismic slip rate V_o measured by *Louie et al.* [1985], 0.5 mm/yr .

DISCUSSION

Any relation to describe the nature of afterslip accumulation with time has to derive from some form of viscous rheology [e.g., *Wesson*, 1988]. In the present modeling we employ rate/state variable constitutive laws, on the basis of their success in describing laboratory and field observations of

frictional phenomena. In the context of this class of constitutive laws, it is important to note that afterslip can only occur on faults that contain a region of velocity-strengthening behavior. For a fault zone that exhibits only velocity-weakening behavior, the steady state frictional resistance decreases with slip velocity, eliminating the stress transient needed to drive afterslip. One could argue that stress transients could be produced with velocity weakening if coseismic slip were small compared with D_c (i.e., if slip ceased during the initial stress increase upon an increase in velocity, Figure 4), however, D_c is thought to be on the order of 10 mm, whereas coseismic offsets are at least an order of magnitude larger for earthquakes of magnitude ≥ 6. Changes in normal stress along a fault during coseismic slip might also contribute to afterslip; however, this would require a very specific ambient stress field and fault orientation, which seems unlikely in view of the generality of afterslip behavior among different faults.

The model presented here is supported by its ability to explain common observations relating to afterslip. One such observation is that of buried slip, or delayed afterslip, such as reported for the 1966 Parkfield earthquake [Smith and Wyss, 1968; Scholz et al., 1969]. The results shown in Figure 6 indicate that for typical values of rise time and the constitutive parameter $a-b$, coseismic surface slip is not expected for velocity strengthening regions thicker than 1-2 km. Thus, since our modeling indicates that $h = 2-4$ km, it is expected that coseismic slip will not break the surface, resulting in buried slip.

A second observation is the relationship between coseismic slip and afterslip and the correlation between the depth to basement and afterslip magnitude, such as reported by Burford [1972], Bucknam et al. [1978], and Williams and Magistrale [1989]; Williams and Magistrale also review a number of earlier examples in southern California. This is predicted by the model, as shown in Figure 6. Areas of locally lower h experience greater coseismic slip and lesser afterslip, for a given earthquake. In southern California, h is controlled by the thickness of the unconsolidated sediments, which overlie the basement, and Williams and Magistrale's data combined with the crustal structure of Fuis et al. [1982] show a good correlation between afterslip and h. In other regions, such as central California, the velocity strengthening region consists of a zone of unconsolidated gouge within the fault. In these cases, along-strike variations in h may be controlled by the pinch and swell of the gouge zone due to roughness of the fault [e.g., Scholz and Aviles, 1986; Power et al., 1987], since narrower areas may be expected to undergo induration and consolidation more quickly, leading to velocity weakening behavior [Dieterich, 1981; Tullis et al., 1989].

Model Parameters

The parameters given by fitting our afterslip relation to data compare well with independent estimates. In the case of $a-b$, the values are fairly tightly constrained by laboratory measurements [Marone et al., 1990], giving values for the depth of the velocity strengthening region of 2-4 km for Parkfield and 2.5-5 km for Superstition Hills (Figures 9 and 11). In both cases, these values agree with those given by independent estimates, providing a check on the appropriateness of using laboratory values for this parameter.

The modeling also provides an estimate of the thickness-averaged coseismic slip velocity and offset (Tables 2 and 3). The values of coseismic offset obtained from fitting data with equation (6) (Table 3) are in good agreement with those of Agnew and Wyatt [1989], which were derived from coseismic strain measurements, and the earliest field measurements [Williams and Magistrale, 1989]. The V^s_{cs} values are somewhat more complicated because they trade off with U^s_c (equations (5) and (6) and Table 3) and because data at very early times are unavailable. Differentiating equation (5) with respect to time and setting $t=0$ shows that, as expected, the afterslip rate should equal the coseismic slip rate at $t=0$. With or without the coseismic slip term, our thickness-averaged values of V^s_{cs} are considerably lower than those of Archuleta [1984]. This may be due to the very short duration of coseismic slip at the surface or to inertial effects not taken into account by our model.

Because of the proximity of the magnitude 6.2 Elmore Ranch earthquake, only 12 hours prior to the Superstition Hills event, we considered the possibility that the misfit for site 2U (Figure 11) was the result of slip triggered by the Elmore Ranch event. Modeling with a more complex relation to account for two overlapping episodes of afterslip showed improved fits, but not sufficiently better to warrant detailed study.

Creep Events

Although we have focused on the overall behavior of afterslip, in detail, afterslip is composed of discreet creep events. While the present model cannot address such features directly, it is worth asking whether they can be understood in the context of rate and state variable friction laws. The question has been addressed in the work of Rice and Gu [1983, p. 209], who in referring to "..transient slip motion, which speeds up, relieves stress, and gradually relaxes without seismic expression.." report that "..this sort of transiently accelerated but aseismic fault slip is the only type of interesting aftereffect possible on fault segments with velocity strengthening..". Rice and Gu's [1983] Figure 9b shows an accelerated slip rate following a sudden increase in stress, such as produced by the passing of a rupture front within a velocity strengthening region.

In connection with creep events, a similar initial increase in stress/slip rate would result from localized failure within the velocity strengthening region, producing a small increment of aseismic slip. The magnitude of such creep events is controlled by the size of the failed region, which depends upon the local stiffness and the constitutive parameters $a-b$ and D_c. Bilham's [1989] data show that the average creep event size remains constant with time after the mainshock. Thus, the overall decay in afterslip with time is caused by an increase in the interevent time. This is to be expected if the stiffness and constitutive parameters of the fault zone material are constant through time, since the stress [or slip rate] increase associated with each localized failure episode will then be constant, producing a characteristic creep event size.

CONCLUSIONS

The model presented here indicates that in accord with a number of other observations of earthquake mechanics, afterslip can be explained as a manifestation of rate/state variable friction behavior within fault zones. Our model is based on a fault zone in which a region of velocity

strengthening frictional behavior overlies a region of velocity weakening (within which earthquakes nucleate). Afterslip is driven by a stress perturbation within the velocity strengthening region, which arises from the increased slip rate associated with rupture propagation from below. Thus the model provides an explanation for the coupling between afterslip and coseismic slip such as indicated by buried slip and modeling showing rapid upward decreases in coseismic slip. That is, afterslip is driven by a stress perturbation that builds as rupture is arrested; both afterslip and the stress perturbation arising from velocity-strengthening frictional behavior.

We derive an afterslip relation based on this model and a 1 degree-of-freedom approximation to elastic interactions between the fault and its surroundings and find that the relation satisfactorily fits afterslip measurements using typical values for the relevant constitutive and seismic parameters. We also fit the model to afterslip measurements to derive best fit values of the constitutive parameter a-b, the thickness of the velocity-strengthening region, and the coseismic slip and velocity. The values so obtained are in good agreement with independent estimates from laboratory experiments and seismic modeling. Our modeling indicates that the depth of the velocity-strengthening region is 2-4 km for the Parkfield region and 2.5-5 km for the Superstition Hills region. The results of recent laboratory friction experiments [*Marone et al.*, 1990] and seismic observations [*Crook*, 1984; *Doser and Kanamori*, 1986, *Marone and Scholz*, 1988] indicate that velocity strengthening is expected within unconsolidated sediments and fault gouge/breccia. In the context of the present model, faults that have no shallow velocity strengthening region (those that do not cut through unconsolidated alluvium or contain a significant ($\approx$ >500 m) gouge/breccia zone) should not exhibit appreciable afterslip.

APPENDIX

A derivation of equation (5) is given here, based on that presented by *Scholz* [1990]. The basis for (5) is the idea that afterslip results from relaxation of a stress pertubation that arises when an earthquake propagates up into a region of velocity-strengthening frictional behavior. The driving force for afterslip derives from the slip rate dependence of friction (Figure 4). We make the assumption that a steady state friction level is achieved during coseismic slip, which for the one-dimensional model presented above, is equivalent to requiring a thickness-averaged coseismic displacement > D_C within the velocity-strengthening region. The driving force for afterslip is given by $\Delta\tau$ (Figure 4, equation (1)).

Afterslip is assumed to obey rate and state variable friction and thus from the definition of the friction rate parameter, we may write an equation relating the postseismic slip velocity V_p the preseismic slip velocity V_0 and the driving force $\Delta\tau$

$$\Delta\tau = (A-B) \ln(V_p/V_0). \qquad (A1)$$

Note that the initial value (at the end of coseismic slip) of V_p is V^s_{cs}. The driving force $\Delta\tau$ decreases with each increment of afterslip, which may be written:

$$\Delta\tau = \tau_c - U_p k, \qquad (A2)$$

where τ_c is the initial value of the driving force (equation (A1)) and k is the spring constant as defined above. Using (A1) to eliminate $\Delta\tau$ and rearranging yields

$$\frac{dU_p}{dt} = V_0 \exp\left\{\frac{\tau_c - U_p\ k}{A-B}\right\}, \qquad (A3)$$

which upon separation of variables and integration leads to equation (5):

$$U_p = \frac{A-B}{k}\ln\left[\left(\frac{kV^s_{cs}}{A-B}\right)t + 1\right], \qquad (A4)$$

If long-term creep continues during [in addition to] afterslip it may be appropriate to add the term $V_0\ t$:

$$U_p = \frac{A-B}{k}\ln\left[\left(\frac{kV^s_{cs}}{A-B}\right)t + 1\right] + V_0\ t. \qquad (A5)$$

Note added in proof. The strong-motion waveform inversion results of *Wald et al.*, [1990] for the 1987 Superstition Hills earthquake show substantial reduction in coseismic slip at 3-5 km, with little coseismic slip occurring above this depth. As do modeling results of the 1979 Imperial Valley event [*Archuleta*, 1984; *Quin*, 1990], *Wald et al.*'s results indicate the existence of a 3-5 km thick velocity strengthening region in the Superstition Hills area. Their results support 1) the general model we use in which afterslip is caused by rupture propagation into a shallow velocity strengthening region (Figure 1) and 2) the results of our afterslip modeling, which indicate a velocity strengthening region 3-5 km thick in the vicinity of Superstition Hills (Figure 12).

REFERENCES

Agnew, D.C., and F. K. Wyatt, The 1987 Superstition Hills earthquake sequence: Strains and tilts at Piñon Flat observatory, *Bull. Seismol. Soc. Am.*, *79*, 480-492, 1989.

Archuleta, R. J., A faulting model for the 1979 Imperial Valley earthquake, *J. Geophys. Res.*, *89*, 4559-4585, 1984.

Biegel, R. L., C. G. Sammis, and J. H. Dieterich, The frictional properties of a simulated gouge with a fractal particle distribution, *J. Struct. Geol.*, *11*, 827-846, 1989.

Bilham, R., Surface slip subsequent to the 24 November 1987 Superstition Hills, California, earthquake monitored by digital creepmeters, *Bull. Seismol. Soc. Am.*, *79*, 424-450, 1989.

Brace, W. F., and J. D. Byerlee, California earthquakes: Why only shallow focus?, *Science*, *168*, 1573-1575, 1970.

Bucknam, R. C., G. Plafker, and R. V. Sharp, Fault movement [afterslip] following the Guatemala earthquake of February 4, 1976, *Geology*, *6*, 170-173, 1978.

Burford, R. O., Continued slip on the Coyote Creek fault after the Borrego Mountain earthquake, in The Borrego Mountain Earthauake of April 9, 1968, *U.S. Geol. Surv. Prof. Pap.*, *787*, 105-111, 1972.

Clark, M. M., R. V. Sharp, R. O. Castle, and P. W. Harsh, Surface faulting near Lake Oroville, California, in August 1975, *Bull. Seismol. Soc. Am.*, *66*, 1101-1110, 1976.

Crook, C.N., Geodetic measurements of horizontal crustal deformation associated with the October 15, 1979 Imperial Valley California earthquake, Ph. D. thesis, 240 pp., Univ. of London, 1984.

Crook, C.N., R. G. Mason, and P. R. Wood, Geodetic measurements of horizontal deformation on the Imperial fault, inThe Imperial Valley Earthquake of October 15, 1979, *U.S. Geol. Surv. Prof. Pap.*,*1254*, 183-191, 1982.

Crough, S. T., and R. O. Burford, Empirical law for fault-creep events, *Tectonophysics*, *42*, T53-T59, 1977.

Dieterich, J. H., Modeling of rock friction, 1, Experimental results and constitutive equations, *J. Geophys. Res.*, *84*, 2161-2168, 1979.

Dieterich, J. H., Constitutive properties of faults with simulated gouge, in *Mechanical Behavior of Crustal Rocks, Geophys. Monogr.*

Ser. vol. 24, edited by N.L. Carter, M. Friedman, J. M. Logan, and D. W. Sterns, pp. 103-120, AGU, Washington, D.C., 1981.

Doser, D. I., and H. Kanamori, Depth of seismicity in the Imperial Valley region 1977-1983 and its relationship to heat flow, crustal structure, and the October 15, 1979, earthquake, J. Geophys. Res., 91, 675-688, 1986.

Fuis, G. S., W. D. Mooney, J. H. Healey, G. A. McMechan, and W. J. Lutter, Crustal structure of the Imperial Valley region, in The Imperial Valley Earthquake of October 15, 1979, U.S. Geol. Surv. Prof. Pap,, 1254, 25-50, 1982.

Gu, J.-C., J. R. Rice, A. L. Ruina, and S. T. Tse, Slip motion and stability of a single degree of freedom elastic system with rate and state dependent friciton. J. Mech. Phys. Solids, 32, 167-196, 1984.

Harsh, P. W., Distribution of afterslip along the imperial fault, in The Imperial Valley Earthquake of October 15, 1979, U.S. Geol. Surv. Prof. Pap., 1254, 193-203, 1982.

Johnson, T. L., and C. H. Scholz, Dynamic properties of stick-slip friction of rock, J. Geophys. Res., 81, 881-888, 1976.

Lorenzetti, E., and T. E. Tullis, Geodetic predictions of a strike-slip fault model: Implications for intermediate- and short-term earthquake prediction, J. Geophys. Res., 94, 12,343-12,361, 1989.

Louie, J. N., C. L. Allen, D. C. Johnson, P. C. Haase, and S. N. Cohn, Fault slip in southern California, Bull. Seismol. Soc. Am., 75, 811-833, 1985.

McNally, K. C., T. Lay, M. Protti-Quesada, G. Valensise, D. Orange, and R. S. Anderson, Santa Cruz Mountains [Loma Prieta] earthquake, Eos Trans. AGU., 70, 1463, 1989.

Marone, C., and C. H. Scholz, The depth of seismic faulting and the upper transition from stable to unstable slip regimes, Geophys. Res. Lett., 15, 621-624, 1988.

Marone, C., C. B. Raleigh, and C. H. Scholz, Frictional behavior and constitutive modeling of simulated fault gouge, J. Geophys. Res., 95, 7007-7025, 1990.

Nason, R.D., Fault creep and earthquakes on the San Andreas fault, in Proc. Conf. Tectonic Probs. San Andreas Fault System., Edited by R.L. Kovach, A. Nur, Stanford Univ. Publ. Geol. Sci., 13, 275-285, 1973.

Nason, R. and J. Weertman, A dislocation theory analysis of fault creep events, J. Geophys. Res., 78, 7745-7751, 1973.

Okubo, P. G., and J. H. Dieterich, Effects of physical fault properties on frictional instabilities produced on simulatd faults, J. Geophys. Res., 89, 5815-5827, 1984.

Okubo, P. G., Dynamic rupture modeling with laboratory-derived constitutive relations, J. Geophys. Res., 94, 12,321-12,335, 1989.

Power, W. L., Tullis, T. E., S. R. Brown, G. N. Boitnott, and C. H. Scholz, Roughness of natural fault surfaces, Geophys. Res. Lett., 14, 29-32, 1987.

Quin, H., Dynamic stress drop and rupture dynamics of the October 15, 1979 Imperial Valley earthquake, Tectonophysics, 175, 93-117, 1990.

Rice, J. R., and J.-C. Gu, Earthquake aftereffects and triggered seismic phenomena, Pure Appl. Geophys., 121, 187-219, 1983.

Ruina, A., Slip instability and state variable friction laws, J. Geophys. Res., 88, 10,359-10,370, 1983.

Scholz, C.H., The critical slip distance for seismic faulting, Nature, 336, 761-763, 1988.

Scholz, C.H., The Mechanics of Earthquakes and Faulting, Cambridge University Press, New York, 1990.

Scholz, C.H., M. Wyss, and S. W. Smith, Seismic and asismic slip on the San Andreas fault, J. Geophys. Res., 74, 2049-2069, 1969.

Scholz, C.H., and C. A. Aviles, The fractal geometry of faults and faulting, in Earthquake Source Mechanics, Geophys. Monogr. Ser. vol. 37, edited by S. Das, J. Boatwright, and C. H. Scholz, pp. 147-156, 1986.

Schulz, S. S., G. M. Mavko, R. O. Burford, and W. D. Stuart, Long-term fault creep observations in central California, J. Geophys. Res., 87, 6977-6982, 1982.

Sharp, R. V., and J. L. Saxton, Three-dimensional records of surface displacement on the Superstition Hills Fault Zone associated with the earthquakes of 24 November 1987, Bull. Seismol. Soc. Am., 79, 376-389, 1989.

Sharp, R. V., et al., Surface faulting in the central Imperial Valley, in The Imperial Valley Earthquake of October 15, 1979, U.S. Geol. Surv. Prof. Pap., 1254, 119-144, 1982.

Sharp, R. V., et al., Surface faulting along the Superstition Hills fault zone and nearby faults associated with the earthquakes of 24 November 1987, Bull. Seismol. Soc. Am., 79, 252-281, 1989.

Smith, S. W., and M. Wyss, Displacement on the San Andreas fault subsequent to the 1966 Parkfield earthquake, Bull. Seismol. Soc. Am., 58, 1955-1973, 1968.

Stuart, W. D., Forecast model for great earthquakes at the Nankai trough subduction zone, Pure Appl. Geophys., 126, 619-641, 1988.

Tse, S. T., and J. R. Rice, Crustal earthquake instability in relation to the depth variation of frictional slip properties, J. Geophys. Res., 91, 9452-9472, 1986.

Tse, S. T., R. Dmowska, and J. R. Rice, Stressing of locked patches along a creeping fault, Bull. Seismol. Soc. Am., 75, 709-736, 1985.

Tullis, T. E., and J. D. Weeks, Constitutive behavior and stability of frictional sliding of granite, Pure Appl. Geophys., 124, 383-414, 1986.

Tullis, T. E., M. L. Blanpied, and J. D. Weeks, The velocity dependence of granite friction with and without simulated gouge, Eos Trans. AGU, 70, 1302, 1989.

Wald, D. J., D. V. Helmberger, and S. H. Hartzell, Rupture process of the 1987 superstition hills earthquake from the inversion of strong-motion data, Bull. Seismol. Soc. Am., 80, 1079-1098, 1990.

Wesson, R. L., Modelling aftershock migration and afterslip of the San Juan Bautista, California, earthquake of October 3, 1972, Tectonophysics, 144, 215-229, 1987.

Wesson, R. L., Dynamics of fault creep, J. Geophys. Res., 93, 8929-8951, 1988.

Williams, P. L., and H. W. Magistrale, Slip along the Superstition Hills fault associated with the 24 Novermber 1987 Superstition Hills, California, earthquake, Bull. Seismol. Soc. Am., 79, 390-410, 1989.

Wong, T.-f., and Y. Zhao, Effects of load point velocity on frictional instability behavior, Tectonophysics, 175, 177-195, 1990.

R. Bilham, CIRES, University of Colorado, Boulder, CO 80302.

C. J. Marone, Department of Geology and Geophysics, University of California, Berkeley, CA 94720

C. H. Scholz, Lamont-Doherty Geological Observatory, Palisades, NY 10964.